

OPEN ACCESS

EDITED BY Haiyang Tang, University of Arizona, United States

REVIEWED BY
Matthew McGraw,
University of Rochester Medical Center,
United States
Md Shadab Ali,
All India Institute of Medical Sciences, India

*CORRESPONDENCE

RECEIVED 23 July 2025 REVISED 30 October 2025 ACCEPTED 03 November 2025 PUBLISHED 28 November 2025

CITATION

Wang H, Jiang W, Xiao J, Geng Y, Ye Q and Ge W (2025) Diacetyl-induced bronchiolitis obliterans involves ubiquitin C upregulation and fibrosis-related gene activation in rats. *Front. Pharmacol.* 16:1671557. doi: 10.3389/fphar.2025.1671557

COPYRIGHT

© 2025 Wang, Jiang, Xiao, Geng, Ye and Ge. This is an open-access article distributed under the terms of the Creative Commons Attribution License (CC BY). The use, distribution or reproduction in other forums is permitted, provided the original author(s) and the copyright owner(s) are credited and that the original publication in this journal is cited, in accordance with accepted academic practice. No use, distribution or reproduction is permitted which does not comply with these terms.

Diacetyl-induced bronchiolitis obliterans involves ubiquitin C upregulation and fibrosis-related gene activation in rats

Hailian Wang¹, Wen Jiang², Junchao Xiao¹, Yan Geng¹, Qing Ye³ and Wei Ge⁴*

¹The Department of Pediatrics, The Second Hospital of Shandong University, Jinan, Shandong, China, ²Department of Central Laboratory, The Second Hospital of Shandong University, Jinan, Shandong, China, ³Department of General Practice, The Second Hospital of Shandong University, Jinan, Shandong, China, ⁴Department of Pediatrics, Qilu Hospital of Shandong University, Jinan, Shandong, China

Introduction: Bronchiolitis obliterans (BO) is an irreversible, chronic obstructive pulmonary disease with inflammation and fibrosis causing bronchiolar narrowing. Inhaling diacetyl (DA) can result in BO in humans.

Methods: We aimed to investigate the relationship between fibrosis-related gene expression and ubiquitin C (UbC) regulation in a rat model of BO following a single DA instillation, by examining lung histopathology, UbC protein levels, and transcriptomic changes.

Results: After DA exposure, rat bronchioles exhibited marked inflammation, increased collagen deposition, airway fibrosis, and obstruction. These changes were confirmed by histology and semi-quantitative image analysis. UbC protein levels were significantly elevated in a time-dependent manner. RNA sequencing revealed significant alterations in gene expression and enrichment of multiple molecular functions and biological processes in BO rats compared with controls, including pathways related to fibrosis formation and ubiquitin dysregulation. Quantitative PCR (qPCR) validation further confirmed the transcriptomic results, showing significant upregulation of Ube2t and Fap and downregulation of Cyp1a1, consistent with enhanced ubiquitin activity, fibroblast activation, and impaired oxidative stress regulation.

Discussion: These findings indicate that DA instillation induces early BO-like changes, disrupts ubiquitin regulation, and increases UbC expression, potentially through oxidative stress—related mechanisms. A better understanding of ubiquitin regulation (particularly UbC) may provide novel molecular targets for therapeutic intervention in BO.

KEYWORDS

bronchiolitis obliterans, diacetyl, fibrosis, ubiquitin C, airway injury

1 Introduction

Bronchiolitis obliterans (BO), also known as obliterative bronchiolitis, is a rare chronic obstructive lung disease characterized by airflow limitation resulting from bronchiolar stenosis and fibrosis. Lung function may gradually progressively deteriorate (Bar et al., 2014). Common causes of BO include inhalation of hazardous fumes, respiratory infections, connective tissue disorders, and complications following lung, heart, or bone marrow transplantation (Aguilar et al., 2016; Lynch et al., 2012). Diagnosis typically involves high-

resolution computed tomography (CT), pulmonary function testing, and, in some cases, lung biopsy (Silva and Müller, 2008).

Industrial inhalants are another major cause of BO. About 2 decades ago, workers in a microwave popcorn factory exposed to butter flavoring vapors developed 'popcorn worker's lung,' a form of BO (Schachter, 2002; Sauler and Gulati, 2012; Harber et al., 2006). Similar cases have been reported among workers in coffee and flavoring industries. The principal toxic agents identified were 2,3-butanedione (diacetyl, DA) and the structurally related 2,3-pentanedione, both of which disrupt airway epithelial integrity, alter protein homeostasis, and induce bronchiolar fibrosis in animal models (Harber et al., 2006; Kreiss, 2017; Hubbs et al., 2019). More recently, DA and related diketones have been detected in most commercial e-cigarette liquids, raising renewed concerns about their potential role in airway injury among vapers (Landman et al., 2019; Allen et al., 2015).

Ubiquitin is an evolutionarily conserved protein that covalently attaches to substrates via its C-terminal glycine residue, regulating protein degradation, localization, and signaling. The ubiquitination cascade involves three key enzymes: ubiquitin-activating (E1), ubiquitination-conjugating (E2), and ubiquitin ligases (E3) enzymes. Through post-translational modification, ubiquitination governs the ubiquitin-proteasome system (UPS), which controls proteolysis, mitosis, and cellular homeostasis (Dastsooz et al., 2019; Chaugule and Walden, 2016; Buetow and Huang, 2016; Spratt et al., 2014). K48-linked chains target proteins for proteasomal degradation, while K63-linked chains can mediate autophagy or signaling (Swatek and Komander, 2016). Dysregulation of ubiquitination has been implicated in various diseases, including cancer and fibrotic disorders (Perrotta et al., 2012; Villegas-Ruiz and Juarez-Mendez, 2016; Wang et al., 2017). Overexpression of E2-related genes such as UBE2C can lead to chromosomal instability and abnormal cell proliferation (van Ree et al., 2010). UbiquitinC (UbC) is one of four ubiquitin-encoding genes (Marinovic et al., 2002). It encodes a stress-inducible polyubiquitin precursor, highly sensitive to ultraviolet radiation, oxidative stress, and translational inhibition, and plays an important role in maintaining ubiquitin homeostasis (Radici et al., 2013; Ryu et al., 2007). Recent studies indicate that dysregulation of the ubiquitin-proteasome system contributes to pulmonary fibrosis and chronic lung injury by disrupting proteostasis and extracellular matrix turnover (Zhang et al., 2025; Lee et al., 2023; Chen et al., 2024). However, the specific role of UbC regulation in the fibrotic remodeling of BO remains unclear.

Therefore, this study aimed to investigate the relationship between fibrosis-related gene expression UbC activation in a rat

Abbreviations: BALF, Bronchoalveolar lavage fluid; BO, Bronchiolitis obliterans; Cyp1a1, Cytochrome P450 family 1 subfamily A member 1; involved in oxidative metabolism; DA, Diacetyl; DEGs, Differentially expressed genes; E2, Ubiquitin-conjugating enzyme; Fap, Fibroblast activation protein; marker of fibrosis; GAPDH, Glyceraldehyde-3-phosphate dehydrogenase; GSEA, Gene set enrichment analysis; GO, Gene ontology; H&E, Hematoxylin-eosin; HRP, Horseradish peroxidase; IHC, Immunohistochemistry; KEGG, Kyoto Encyclopedia of Genes and Genomes; PCA, Principal component analysis; PPI, Protein-protein interaction; qPCR, Quantitative polymerase chain reaction; SD, Sprague-Dawley; SQSTM1, Sequestosome-1 (p62) scaffolding protein; UbC, Ubiquitin C; Ube2t, Ubiquitin-conjugating enzyme E2T; WB, Western blot.

model of diacetyl-induced BO. Histopathological evaluation, collagen semi-quantification, and UbC protein analysis were combined with transcriptomic profiling to elucidate the molecular mechanisms linking oxidative stress, ubiquitin dysregulation, and fibrosis. In addition, to validate key transcriptomic findings, representative genes related to ubiquitination (Ube2t), fibrosis (Fap), and oxidative metabolism (Cyp1a1) were selected for quantitative PCR (qPCR) analysis.

2 Materials and methods

2.1 Ethical approval

All data comply with scientific and ethical standards. All animal studies were approved by the Animal Ethics Committee of the Second Hospital of Shandong University, number KYU-2019(KJ) A-0160. Experimental animal management followed the Guide for the Care and Use of Laboratory Animals of the National Institutes of Health.

2.2 Construction of the BO rat model

Male Sprague-Dawley (SD) rats (n = 18, 250-300 g) were purchased from the Wuhan Experimental Animal Center (Wuhan, China). After weighing, they were randomly assigned to a DA instillation group (n = 9) and a control group (n = 9). All rats were observed daily, fed regularly and kept n a routine environment at a temperature of 24 °C \pm 0.5 °C, and humidity of 55% \pm 5%. DA (Sigma, United States) was diluted with physiological saline to a final concentration of 188 mg/mL. On day 1, rats were anesthetized with sodium pentobarbital (50 mg/kg, intraperitoneally) and DA (125 mg/kg) was instilled intratracheally as a single dose. The control group received an equal volume of normal saline. Three rats from each group were anesthetized, subjected to bronchoalveolar lavage fluid (BALF) collection, and then euthanized with an overdose of pentobarbital sodium (150 mg/kg, i.p.) on days 3, 5, and 7 after DA instillation for histopathological and molecular analyses.

2.3 Bronchoalveolar lavage fluid (BALF) measurement

BALF was collected by injection of 1 mL of sterile phosphate buffered saline (PBS) into the rats' lungs, via the trachea, three times, and the total number of cells was counted with a blood cell counter. After centrifugation (for 10 min, at 500 g), the percentages of eosinophils, lymphocytes, and neutrophils were determined using microscopy.

2.4 Tissue sections and hematoxylineosin (H&E)

Lung tissue was dehydrated, and then sequentially immersed in three jars of paraffin (at 60 °C), and the wax-soaked tissue blocks,

wrapped in paraffin, were sliced with a pathological microtome, placed in a 40 °C water bath, and baked at 60 °C for 3 h. The paraffin sections were dewaxed and stained with hematoxylin with eosin then added and then further dehydrated. Finally, the slices were airdried under a fume hood. Neutral gum was added dropwise, slides were then covered with clean coverslips, and examined under a microscope. For collagen quantification, the percentage of collagen fiber area was measured from Masson-stained sections using ImageJ software (NIH, United States), and the mean of three randomly selected microscopic fields per sample was calculated.

2.5 Immunohistochemistry (IHC)

For IHC paraffin sections were dewaxed and EDTA antigen retrieval buffer was added, and heated at 98 °C for 20 min. Hydrogen peroxide 3% was added dropwise to inhibit endogenous peroxidase, and then goat serum added dropwise with incubation for 30 min. The primary antibodies, UbC (Rabbit, Proteintech, United States Cat# 10457-1-AP, dilution 1:1000) and GAPDH (Mouse, Proteintech, United States Cat# 60004-1-Ig, dilution 1:50000), were added and incubated overnight at 4 °C. The following day, horse radish peroxidase (HRP)-labelled goat anti-rabbit secondary antibody (ZSGB, China Cat# ZB-2301, 1:10000) and HRP-labelled goat anti-mouse secondary antibody (ZSGB, China Cat# ZB-2305, 1: 10000) was added dropwise and incubated at 37 °C for 30 min. DAB chromogenic solution was added to each section which was then examined under a microscope. Harris hematoxylin counterstain was used, and after differentiation, sections were immersed in PBS to restore the blue color. After dehydration, until transparent, sections were air-dried, then sliced and sealed using neutral gum. The imaged under a confocal microscope (Olympus BX53)

2.6 Western blot (WB) analysis

Total protein was extracted from cells using lysis buffer for 30 min with centrifugation for protein quantification. The whole cell extract was mixed with Laemmli loading buffer, boiled for 5 min, and then subjected to SDS-PAGE. Proteins were transferred to a PVDF membrane and incubated with specific antibodies UbC (Rabbit, Proteintech, United States Cat# 10457-1-AP, dilution 1: 1000) and GAPDH (Mouse, Proteintech, United States Cat# 60004-1-Ig, dilution 1:50000),. The membrane was washed with Trisbuffered saline and Tween-20 (TBST), and HRP-labelled secondary antibody, was added for 1 h at room temperature. Immune complexes were visualized using the ECL Western Blotting Detection Kit (ZSGB, China).

2.7 RT-qPCR analysis

Total RNA was extracted from lung tissues using the RNeasy Mini Kit (Qiagen United States), and RNA purity and concentration were determined with a NanoDrop 2000 spectrophotometer (Thermo Fisher Scientific, United States) by assessing the A260/A280 ratio. Complementary DNA (cDNA) was synthesized from 1 µg of total RNA using the High-Capacity cDNA Reverse

Transcription Kit (Thermo Fisher Scientific, United States) according to the manufacturer's instructions. Quantitative realtime PCR (RT-qPCR) was performed using 10 ng of cDNA per reaction with PowerTrack™ SYBR Green Master Mix (Thermo Fisher Scientific, United States) on a QuantStudio™ 7 Pro Real-Time PCR System (Applied Biosystems, United States). Each sample was analyzed in triplicate. The thermal cycling conditions were: initial denaturation at 50 °C for 2 min and 95 °C for 10 min, followed by 40 cycles of 95 °C for 15 s and 60 °C for 1 min. Relative gene expression was calculated using the 2-ΔΔCt method, normalizing Ct values of target genes to the endogenous control (GAPDH) and comparing experimental to control groups. Primer sequences were designed using Primer-BLAST (NCBI) and synthesized by Sangon Biotech (Shanghai, China). Primer specificity was verified by melt-curve analysis showing a single amplification peak, and amplification efficiency ranged between 90% and 105%. Details of primer sequences are provided in Table 1.

2.8 RNA isolation and expression analysis

RNA sequencing was performed on lung tissues collected at Day 7 after DA instillation (n = 3 per group). The RNA Nano 6000 Assay Kit for the Bioanalyzer 2100 System (Agilent Technologies, CA, United States) was used to assess RNA integrity. Samples were clustered on a cBot Cluster Generation System with TruSeq PE Cluster Kit v3-cBot-HS (Illumina) following the manufacturer's instructions. Raw data in fastq format were first processed using fastp software. Differential gene expression analysis was performed on the specimens (3 biological replicates per time point) from the two groups using the DESeq2 R software package (1.20.0). Differential expression analysis was also performed using the EdgeR R package (3.22.5). The resulting P values were adjusted for false discovery rates using the Benjamini and Hochberg method. The clusterProfiler R package was used to implement gene ontology (GO) enrichment and Kyoto Encyclopedia of Genes and Genomes (KEGG) analysis of differentially expressed genes. P values less than 0.05 were considered to indicate significant enrichment of differentially expressed genes. Gene set enrichment analysis (GSEA) was performed from the webside (https://www.gseamsigdb.org/gsea/index.jsp). The GO and KEGG datasets were independently used for GSEA. STRING was used to predict protein-protein interactions (https://string-db.org/).

2.9 Statistical analyses

Statistical analyses were performed using GraphPad Prism version 10.0 (GraphPad Software, United States). Differences between two groups were analyzed using the paired t-test, while comparisons among multiple groups were performed using one-way analysis of variance (ANOVA) followed by Tukey's post hoc test. RNA-seq data were analyzed using the DESeq2 package, and the Benjamini–Hochberg false discovery rate (FDR) method was applied to correct for multiple testing. A P value <0.05 was considered statistically significant.

TABLE 1 Primer sequences used for quantitative real-time PCR.

·						
Gene symbol	Accession no.	Forward primer (5'→3')	Reverse primer (5'→3')	Product length (bp)	Annealing Tm (°C)	Source
Ube2t	NM_001108344.2	TGCACATGCTAGCCA TCGAA	CGGATCTGTGGTGGC TCAAA	175	60	This study
Fap	NM_138850.1	CCAGCTGGGAATACT ACGCC	GGTCAGAGTACCACA TCGCC	153	60	This study
Cyp1a1	XM_006243150.4	CAGAGGTTGGCCACT TCGAC	TATGCTGAGCAGCTC TTGGTC	148	60	This study
Gapdh	NM_017008.4	GCATCTTCTTGTGCA GTGCC	GGTAACCAGGCGTCC GATAC	122	60	Housekeeping gene

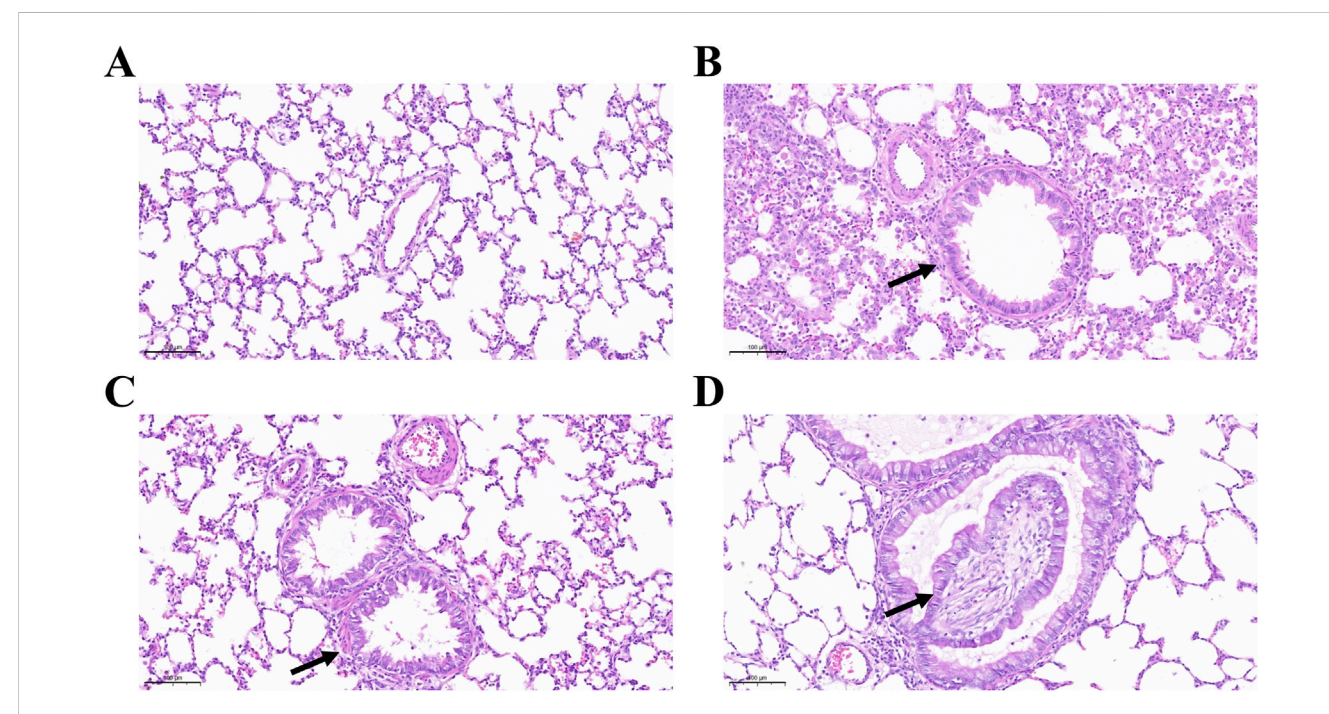


FIGURE 1
Intraluminal fibrosis and obliterative bronchiolitis after diacetyl (DA) instillation. (A) Normal bronchiolar epithelium and airway structure in the normal saline (NS) control group on day 7. (B) Bronchioles showing epithelial hyperplasia on day 3 after DA instillation (black arrow) (Scale bars: 100μm). (C) Bronchioles exhibiting concentric intramural fibrosis and luminal narrowing on day 5 after DA instillation (black arrow) (Scale bars: 100μm). (D) Extensive intraluminal fibrosis on day 7 after DA instillation, with almost complete airway obstruction, marked collagen deposition, and fibrotic remodeling (black arrow) (Scale bars: 100μm).

3 Results

3.1 Histopathologic changes characteristic of BO after DA instillation

During the experiment, rats in the control group remained healthy and showed no abnormal behavior. In contrast, rats in the DA-treated group exhibited signs of lethargy and reduced food intake by day 2, although respiration initially remained unaffected. Their general condition gradually improved over time; however, respiratory symptoms progressively worsened. By day 6, the remaining rats in the DA group developed marked dyspnea accompanied by intermittent coughing.

Figure 1 illustrates the histopathological progression of bronchiolitis obliterans (BO) and intraluminal fibrosis following DA exposure compared with saline controls. As the disease advanced, the loose connective tissue was progressively replaced by dense, mature collagen, leading to airway fibrosis. This resulted in loss of elasticity, impaired expansion and contraction, and diminished regenerative potential. Necrotizing fibrosis adjacent to the airway lumen caused varying degrees of tissue damage, and by day 7, the bronchiolar lumen was almost completely occluded by fibrotic tissue.

Figure 2 shows the development of peribronchial and interstitial inflammation. Compared with the saline group, the DA-treated rats displayed mild to moderate nodular hyperplasia of peribronchial lymphoid tissue on days 3 and 5, which became more diffuse by day 7. Linear hyperplasia and infiltration of mixed inflammatory cells were observed in the interstitial space. Masson's trichrome staining revealed marked collagen deposition, suggesting that epithelial and

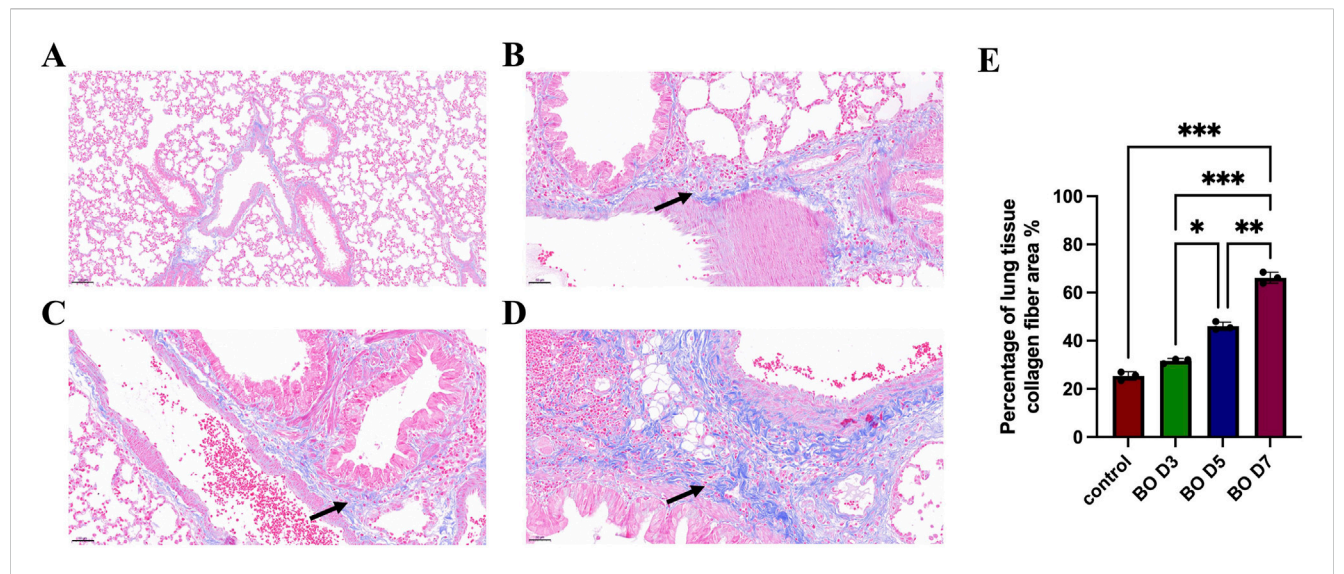


FIGURE 2 Peri-interstitial inflammation in bronchiolitis obliterans following diacetyl (DA) instillation. (A) Normal bronchioles from an NS control rat on day 7 showing intact airway epithelium and architecture (Scale bars: $100 \mu m$). (B) On day 3 after DA instillation, bronchioles display peribronchiolar inflammation and epithelial regeneration with mild hyperplasia (black arrow) (Scale bars: $50 \mu m$). (C) On day 5, bronchioles exhibit more extensive epithelial damage, tissue destruction, and dense infiltration of neutrophils and macrophages within the interstitium (black arrow) (Scale bars: $50 \mu m$). (D) Masson's trichrome staining reveals widespread fibroplasia and interstitial collagen deposition (black arrow), indicating progressive fibrosis and loss of normal bronchiolar structure (Scale bars: $50 \mu m$). (E) Semi-quantitative analysis of collagen deposition. Data are presented as mean \pm SD (n = 3 rats per group per time point). Statistical significance was determined by one-way ANOVA followed by Tukey's post hoc test; P < 0.05 was considered statistically significant. *P < 0.05, **P < 0.01, and ***P < 0.001.

mucosal injury contributed to the development of subsequent fibrosis. Quantitative analysis of collagen deposition showed a progressive increase in collagen fiber area percentage from day 3 to day 7 after diacetyl instillation, consistent with histological evidence of fibrosis.

3.2 Inflammatory cell response in BALF of BO following DA instillation

BALF was examined to determine percentage changes in neutrophils, macrophages, and lymphocytes following DA exposure. Neutrophils increased significantly on days 3, 5, and 7, with statistical differences between the DA instillation and control groups. On day 7, the BALF neutrophilia was significantly higher than on days 5 and 3 after DA instillation $(56.33 \pm 2.52 \text{ vs. } 43.33 \pm 1.53 \text{ vs. } 35.33 \pm 4.93, \text{ Figure 3A})$. By contrast, the percentage of BALF macrophages gradually decreased after DA; on day 7 BALF macrophages were significantly lower than on days 5 and 3 $(20.33 \pm 1.53 \text{ vs. } 33.67 \pm 3.51 \text{ vs. } 40.33 \pm 1.53, \text{ Figure 3B})$. BALF lymphocytes were significantly decreased on day 7 after DA instillation compared to saline control $(20.33 \pm 2.31 \text{ vs. } 34.33 \pm 3.51)$ but there were no significant differences on days 3 and 5 (Figure 3C).

3.3 Increased expression of UbC in BO after DA instillation

After instillation of DA, UbC protein expression on WB of rat lungs increased significantly, compared to the saline control group, on days 3, 5, and 7 (1.49 \pm 0.02 vs. 1.63 \pm 0.05 vs. 2.1 2 \pm 0.04, Figures 3D,E).

Increased UbC protein expression was observed on lung tissue sections in the intrapulmonary airways, gradually increasing after DA instillation; but was seen only rarely in controls (Figure 3F).

3.4 Identification of differentially expressed genes in BO after DA instillation

Transcriptomic profiling was performed using Day 7 samples, which exhibited the most representative histopathological and biochemical features of BO. mRNA sequencing was employed to investigate transcriptomic alterations induced by DA exposure. Principal component analysis (PCA) revealed distinct transcriptomic separation between the DA-treated and saline control groups (Figure 4B). Hierarchical clustering heat maps demonstrated consistent expression patterns within each group (Figure 4A). Compared with the saline control group, transcriptomic profiling of BO rats revealed the overall distribution of expressed genes, with 1,474 genes showing increased expression, 367 showing decreased expression, and the remainder exhibiting no significant change (Figure 4C).

Functional enrichment analysis of DEGs was performed using the ClusterProfiler R package. Gene Ontology (GO) analysis revealed significant enrichment of genes associated with microtubule motor activity, tubulin binding, microtubule organization, and ciliary structure and movement, including "supramolecular fiber," "motile cilium," and "microtubule bundle formation" (Figure 5A). Kyoto Encyclopedia of Genes and Genomes (KEGG) pathway analysis further showed enrichment of genes involved in neuroactive ligand–receptor interaction, protein digestion and absorption, PI3K–Akt signaling, cardiac muscle

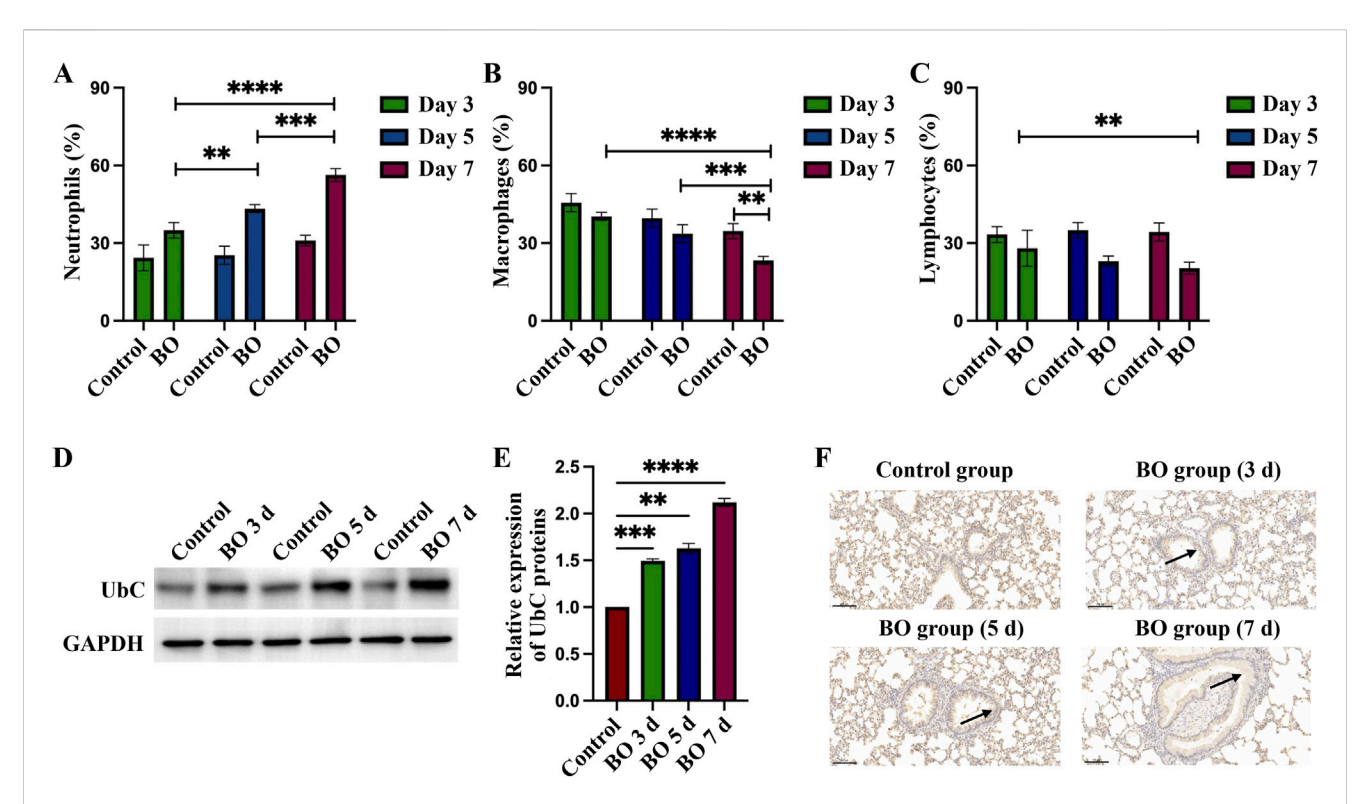


FIGURE 3 Differential cell percentages in BALF and expression of UbC in rats lungs after DA instillation. (A–C) Percentages of neutrophils, macrophages, and lymphocytes in bronchoalveolar lavage fluid (BALF) on days 3, 5, and 7 after DA instillation compared with saline controls. (D) Western blot analysis showing UbC protein expression at 3d, 5d, and 7d following DA instillation or saline treatment. (E) Quantification of UbC protein, normalized to total protein, expressed relative to saline control; (F) Immunohistochemical staining for UbC in lung sections demonstrating enhanced UbC expression in airway epithelial and peribronchial regions after DA exposure (black arrow) (Scale bars: $100 \, \mu m$). Data are presented as mean \pm SD (n = 3 rats per group per time point). Statistical significance was determined by one-way ANOVA followed by Tukey's post hoc test; P < 0.05 was considered statistically significant. **P < 0.001, ***P < 0.001, and ****P < 0.0001.

contraction, hypertrophic cardiomyopathy, ECM-receptor interaction, cell cycle regulation, complement and coagulation cascades, and *Staphylococcus aureus* infection (Figure 5B).

Protein-protein interaction (PPI) network analysis using the STRING database demonstrated strong consistency with the GO and KEGG enrichment results, highlighting interconnected molecular pathways contributing to fibrosis and airway remodeling (Figure 5C).

3.5 Fibrosis-associated and ubiquitin-related gene expression in BO rats after diacetyl exposure

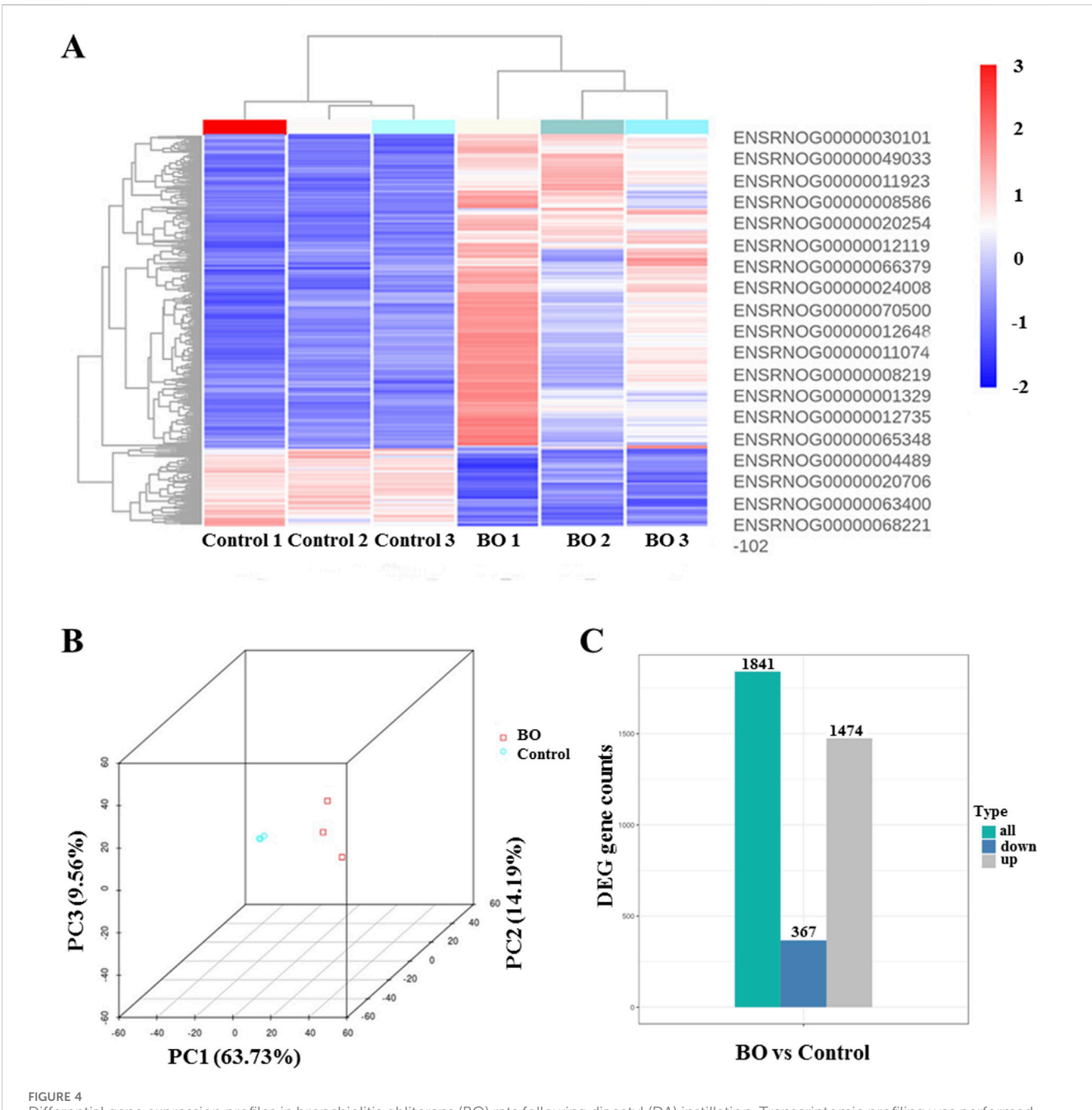
Differential gene analysis and GSEA were performed to explore fibrosis and ubiquitin-associated pathways in bronchiolitis obliterans (BO) rats. A total of 497 genes were upregulated and 81 were downregulated in the DA group compared with saline controls (Padj \leq 0.01, |Log₂FoldChange| \geq 2.0). The top differentially expressed genes identified on Day 7 are listed in Supplementary Table S1.

Among the most upregulated genes were Bpifb2, Myh6, Aqp3, Itln1, R3hdml, while Cyp1a1, Slc26a3, Sirpa1, Chrnb3, and Gstm1 were among the most downregulated (Figure 6A). In addition, genes related to ubiquitin regulation, including Ube2t

and Uchl1, fibrosis-related gene including Fap, showed marked upregulation, suggesting activation of ubiquitin-proteasome and fibrosis-associated signaling. Notably, Cyp1a1—involved oxidative metabolism-was markedly suppressed, consistent with oxidative stress-induced disruption of detoxification pathways. **GSEA** revealed significant enrichment fibroblast proliferation-related gene sets, including "fibroblast proliferation," "regulation of fibroblast proliferation," and "positive regulation of fibroblast proliferation" (Figures 6B-D). In parallel, gene sets related to ubiquitin-protein ligase activity, ubiquitin-like protein ligase binding, regulation of protein ubiquitination, and ubiquitinmediated proteolysis were significantly enriched in the BO group (Figures 7A–D), supporting a central role of ubiquitin dysregulation in fibroblast activation and airway fibrosis.

To validate these transcriptomic findings, qPCR was performed for three representative genes. Consistent with RNA-seq data, Ube2t and Fap were significantly upregulated in a time-dependent manner, while Cyp1a1 was downregulated following DA exposure (P < 0.05, Figure 6E). These results support that DA-induced airway injury involves activation of ubiquitin-related pathways and fibroblast proliferation, contributing to fibrotic airway remodeling.

The results demonstrate that a single intratracheal instillation of diacetyl induces a cascade of pathological changes characterized by inflammatory cell infiltration, progressive collagen deposition, and airway fibrosis expecially day 7. These histological alterations were



Differential gene expression profiles in bronchiolitis obliterans (BO) rats following diacetyl (DA) instillation. Transcriptomic profiling was performed on Day 7 lung tissues from DA-treated and saline control rats (n = 3 per group). (A) Heat map showing representative differentially expressed genes (DEGs) between BO and control groups. Red indicates upregulated genes, and blue indicates downregulated genes. (B) Principal component analysis (PCA) plot demonstrating clear separation between DA-treated and control samples, indicating consistent transcriptomic alterations induced by DA exposure. (C) Overall distribution of differentially expressed genes, summarizing the total number of upregulated and downregulated genes identified in BO compared with controls. Differential expression was analyzed using DESeq2 (padj \leq 0.05, $|\log_2$ FoldChange| \geq 1.0).

accompanied by increased expression of UbC protein and significant transcriptomic changes involving fibrosis-related and ubiquitin-associated genes. The integration of these findings suggests that diacetyl exposure triggers both fibrogenic activation and disruption of ubiquitin-mediated proteostasis, processes that may collectively contribute to the development and persistence of bronchiolitis obliterans. To further interpret these results and their mechanistic implications, we expanded the following Discussion section.

4 Discussion

BO is a rare condition in which airway inflammation and peribronchial fibrosis led to bronchiolar stenosis, concentric narrowing and even complete occlusion. Its histopathologic features include epithelial disruption, bronchiolar smooth muscle hypertrophy, peribronchiolar inflammation and granulation tissue, fibrous tissue hyperplasia, scarring of distal airways and luminal obstruction. Small airways obstruction leads to hyperinflation (air

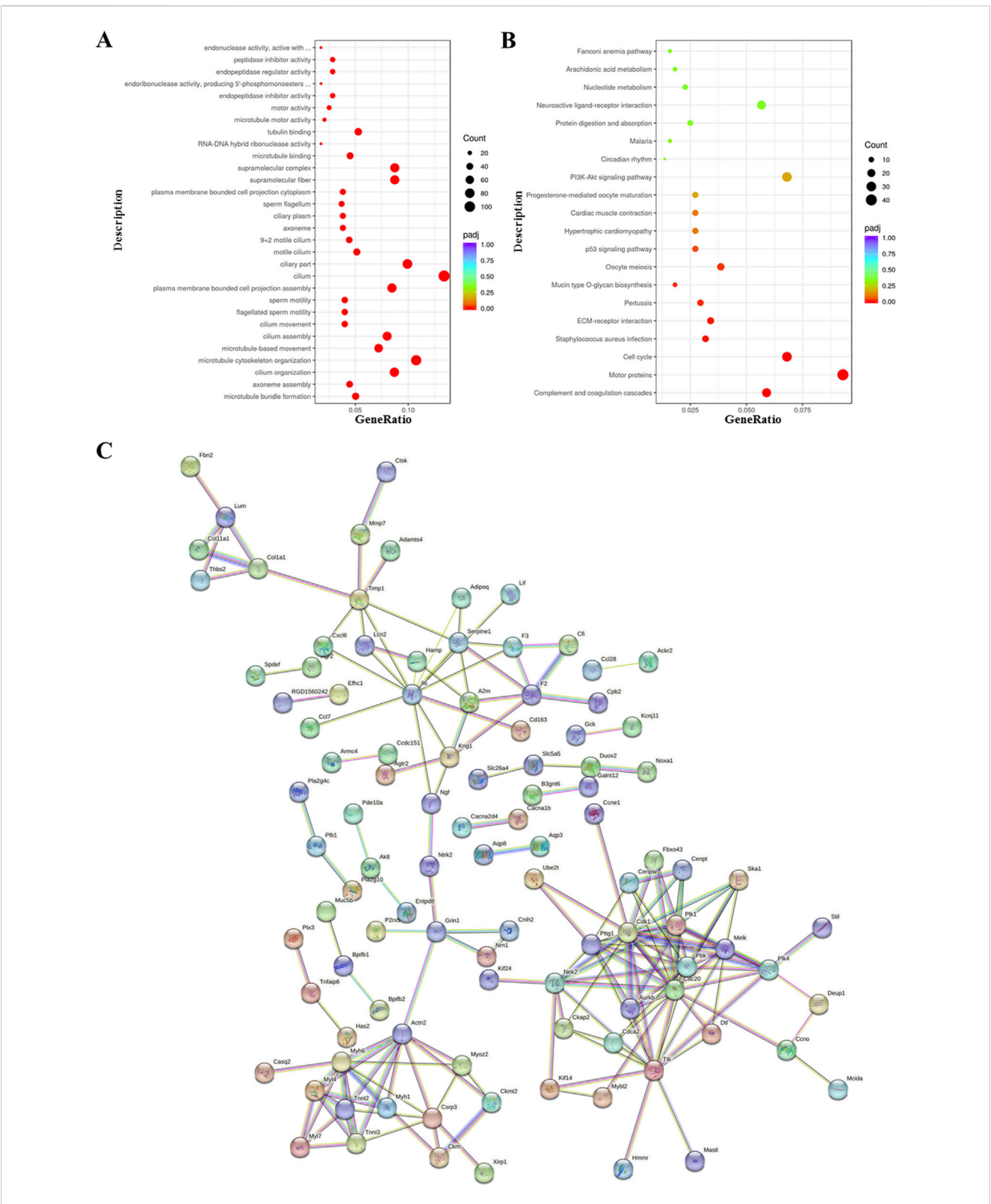
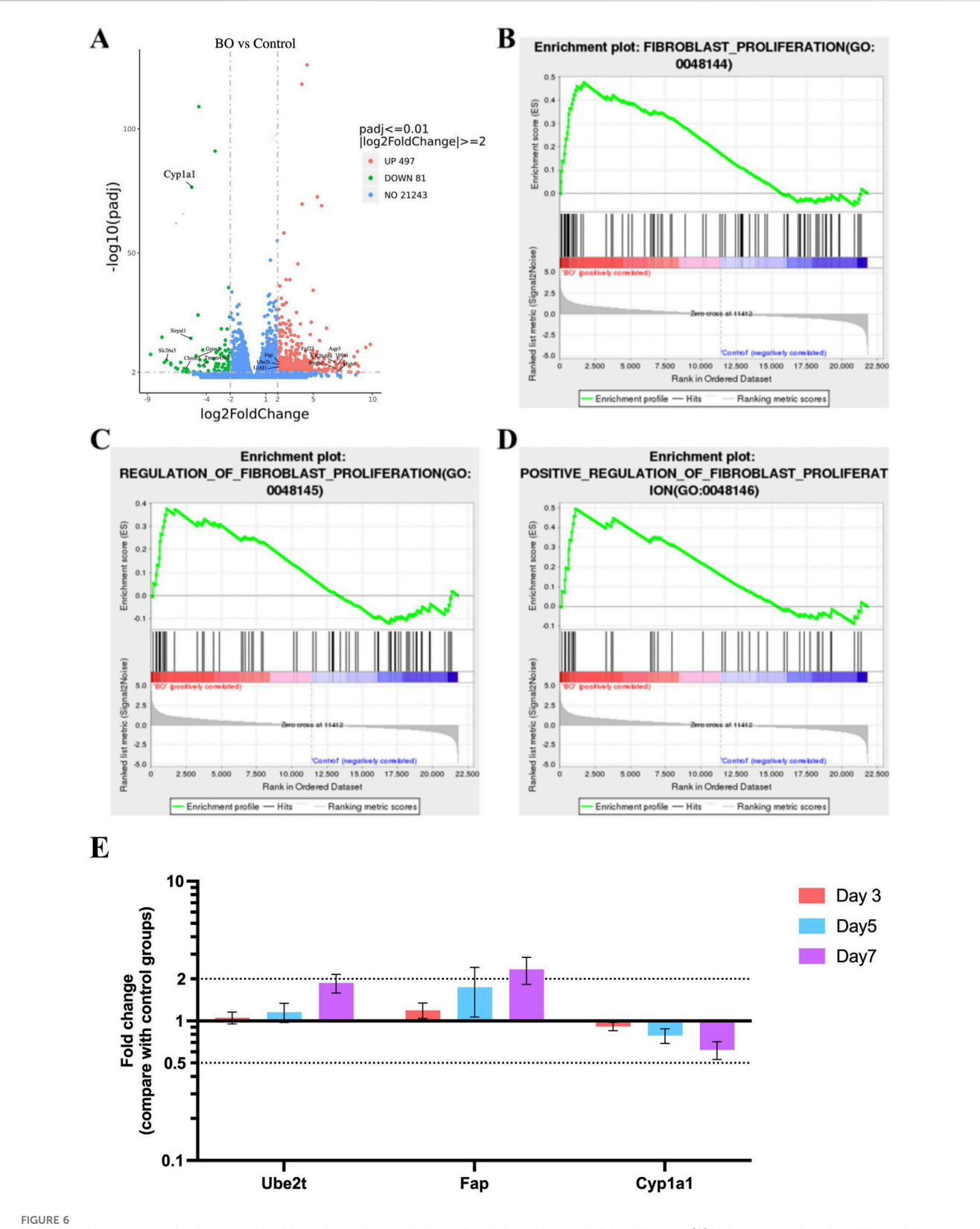


FIGURE 5
Functional enrichment analysis of differentially expressed genes in bronchiolitis obliterans (BO) following diacetyl (DA) instillation. (A) Gene
Ontology (GO) enrichment analysis, showing the 30 most significantly enriched biological terms. (B) Kyoto Encyclopedia of Genes and Genomes (KEGG)
pathway analysis, highlighting the top 20 enriched signaling pathways. (C) STRING protein–protein interaction network, in which nodes represent
upregulated proteins and connecting lines indicate functional associations. For all enrichment analyses, genes with $|\log 2FoldChange| \ge 2$ and
adjusted p < 0.05 were included. In the bubble plots, the x-axis represents the gene ratio, bubble size indicates the number of enriched genes, and bubble
color corresponds to—log10 (adjusted p-value).



Fibrosis -related gene activation and ubiquitin pathway dysregulation in DA-induced bronchiolitis obliterans. (A) Volcano plot showing differentially expressed genes (DEGs) in the BO and saline control groups. Red and green dots represent significantly upregulated and downregulated genes, respectively (padj <0.01, $|\log_2 FoldChange| \ge 2$). The top genes with the greatest $|\log_2 FoldChange|$ are labeled on the plot. (B) Enrichment of the Fibroblast proliferation gene set. (C) Enrichment of the Regulation of fibroblast proliferation gene set. (D) Enrichment of the Positive regulation of fibroblast (Continued)

FIGURE 6 (Continued)

proliferation gene set. **(E)** Quantitative PCR validation of Ube2t, Fap, and Cyp1a1 genes. Data are shown as mean \pm SD (n = 3 rats per group, each sample run in triplicate). Genes with $|\log_2 \text{FoldChange}| \ge 2$ and adjusted p < 0.05 were defined as significantly differentially expressed. Significance was determined by false discovery rate (FDR) < 0.25 and adjusted p < 0.05 after 1,000 permutations. Positive enrichment scores (NES >0) indicate upregulation in DA-treated lungs, while negative scores (NES <0) indicate downregulation.

trapping), patchy atelectasis, with a reduction in blood vessel volume and number, resulting in impaired ventilation and hypoxemia (Kerger and Fedoruk, 2015; Krishna et al., 2024). DA is water-soluble and is readily absorbed through the mucous membranes of the nose, pharynx, larynx and trachea producing an acute inflammatory response and potential damage (Gloede et al., 2011).

Various animal studies have demonstrated that inhalation or tracheal instillation of diacetyl (DA) and its analog 2,3-pentanedione induces airway injury and fibrosis similar to those observed in human bronchiolitis obliterans. Both rat and mouse models have been widely used to explore the mechanisms underlying distal airway inflammation and bronchiolar remodeling (Morgan et al., 2012; Morgan et al., 2008). High concentrations of inhaled DA lead to marked bronchiolar inflammation, epithelial sloughing, and progressive fibrotic changes in the small airways (Krishna et al., 2024). A single intratracheal dose of DA has been shown to reproduce the cardinal histopathological features of BO in rats, including epithelial injury, peribronchial inflammation, and luminal fibrosis (Kreiss, 2014). In the present study, we employed this acute high-dose intratracheal model to achieve reproducible epithelial damage and early fibrotic remodeling, which were consistent with published animal models (Morgan et al., 2012; Morgan et al., 2008; Palmer et al., 2011; Flake and Morgan, 2017) and the pathological manifestations of human BO. While occupational and vaping exposures are typically chronic and lower in concentration, both acute and chronic DA exposures activate similar downstream pathways involving oxidative stress, epithelial injury, ubiquitin dysregulation, and fibroblast-driven fibrosis. This acute model therefore effectively captures the early molecular events, particularly UbC upregulation and disturbance of ubiquitin homeostasis, that initiate the fibrotic remodeling characteristic of BO.

Ubiquitin is encoded by UbC, ubiquitin B (UBB), UBA52, and RPS27A; polyubiquitin-C is another source of ubiquitin. Polyubiquitin-C controls a multitude of biological functions. Under physiological circumstances, it assists maintenance of homeostatic levels of ubiquitin which is stimulated in response to heat shock, oxidative stress, and translational damage (Ki et al., 2010; Snyder and Silva, 2021). UbC is activated during gene transcription and stress and provides excess ubiquitin to remove damaged/unfolded proteins (Ryu et al., 2007). Polyubiquitin-C is involved in a variety of biological processes, including innate immunity, DNA repair, and kinase activity (Rajsbaum et al., 2014; Rajsbaum and García-Sastre, 2014; Tsirigotis et al., 2001; Pickart et al., 2004). In mouse embryonic fibroblasts, the UbC gene was investigated, and homozygous deletion was found to reduce cellular ubiquitin levels and viability under oxidative stress (Ryu and Ryu, 2011). Repetitive inhaled DA was shown to promote ubiquitin proteasomal stress and UbC protein expression (Wang et al., 2021). Following DA inhalation, extensive accumulation of total ubiquitin, K63-ubiquitin, and scaffolding protein sequestome-1 (SQSTM1) puncta in respiratory epithelial cells was demonstrated, indicating severe damage to proteins in the airways. The colocalization of ubiquitin with SQSTM1 and airway epithelial cell lysosomes implies that DA-induced airway damage involves extensive autophagy (Hubbs et al., 2016). We found UbC protein levels were significantly increased 7 days after a single DA administration, suggesting a stress-induced ubiquitin response associated with oxidative injury in BO rats. UbC upregulation appears to represent a stress-induced activation of the ubiquitin-proteasome system, contributing to early regulatory events in fibrotic remodeling. Rather than implying a direct causal role, these findings indicate that UbC may serve as a key adaptive regulator linking oxidative stress, proteostasis imbalance, and fibroblast activation.

To further elucidate the molecular mechanisms underlying these processes, RNA sequencing revealed distinct gene expression profiles in BO rats compared with controls. GO enrichment analysis identified significant alterations in genes involved in microtubule assembly, ciliary function, and extracellular matrix organization, all of which are implicated in fibrosis development. KEGG pathway analysis showed enrichment in PI3K-Akt signaling, ECM-receptor interactions, cell cycle regulation and coagulation pathways, consistent with fibroblast activation and immune dysfunction. GSEA demonstrated enrichment of genes related to fibroblast proliferation, ubiquitin ligase activity, protein ubiquitination, and proteostasis regulation, linking ubiquitin pathway disturbance with fibrotic remodeling.

qPCR validation further confirmed these transcriptomic findings, showing significant upregulation of Ube2t and Fap, and downregulation of Cyp1a1, consistent with enhanced ubiquitin activity, fibroblast activation, and impaired oxidative stress regulation. These genes collectively support the hypothesis that DA exposure simultaneously triggers proteotoxic stress and fibrotic signaling cascades, promoting irreversible airway remodeling.

Taken together, our findings provide a coherent and mechanistically novel model of diacetyl (DA)-induced bronchiolitis obliterans. By combining histopathology, protein analysis, and transcriptomic profiling, we demonstrated for the first time that a single high-dose DA exposure is sufficient to trigger early, reproducible features of bronchiolar fibrosis in rats. Following DA exposure, airway epithelial injury and inflammatory infiltration initiate a fibrotic cascade characterized by collagen deposition and fibroblast activation. At the molecular level, our data reveal a previously unrecognized disturbance of the ubiquitin-proteasome system—marked by UbC upregulation and altered expression of Ube2t and Uchl1—which appears to link

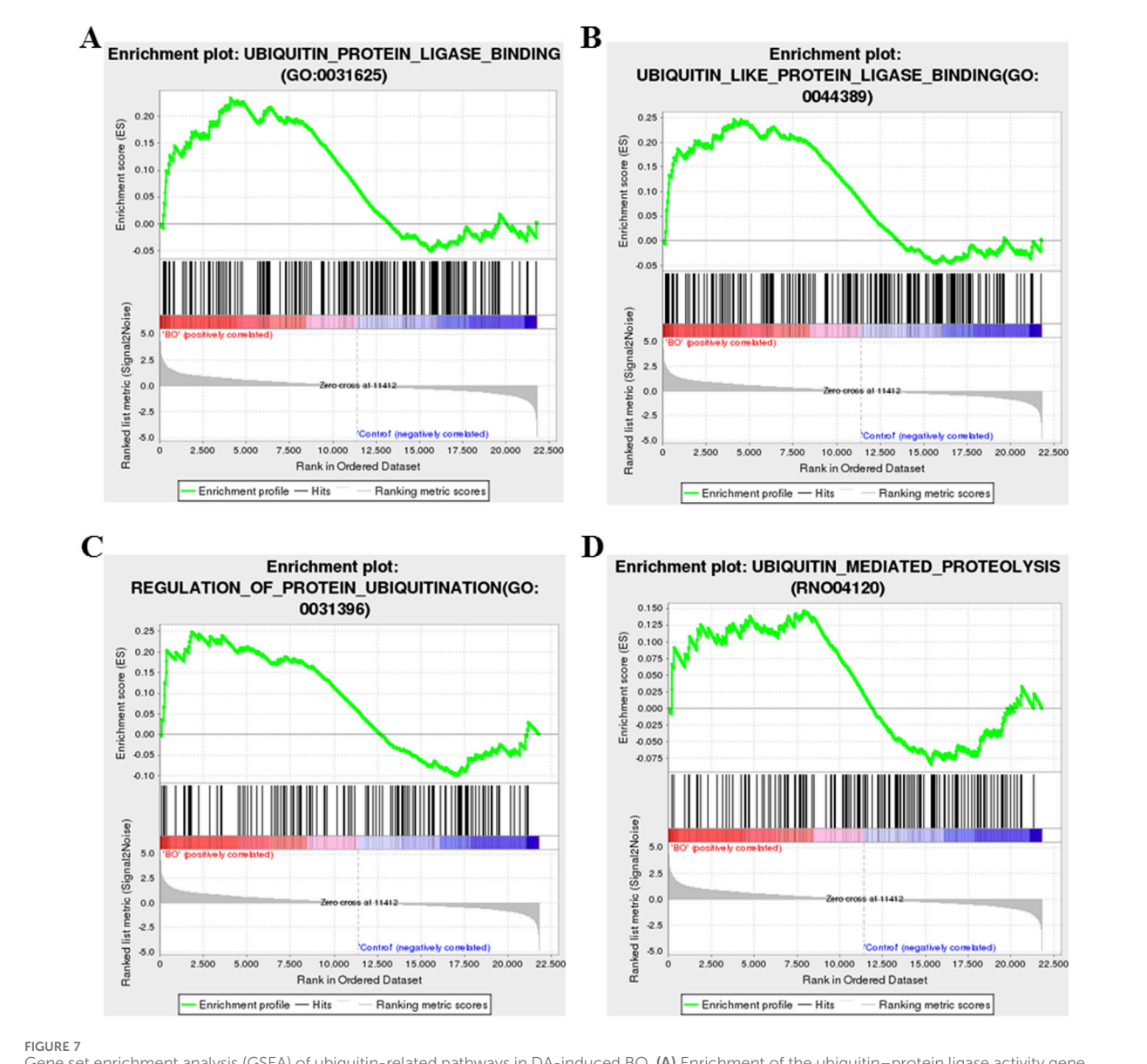


FIGURE 7
Gene set enrichment analysis (GSEA) of ubiquitin-related pathways in DA-induced BO. (A) Enrichment of the ubiquitin-protein ligase activity gene set. (B) Enrichment of the ubiquitin-like protein ligase binding gene set. (C) Enrichment of the regulation of protein ubiquitination gene set. (D) Enrichment of the ubiquitin-mediated proteolysis gene set. Significance was determined by false discovery rate (FDR) < 0.25 and adjusted p < 0.05 after 1,000 permutations. Positive enrichment scores (NES >0) indicate upregulation in DA-treated lungs, while negative scores (NES <0) indicate downregulation.

oxidative stress with fibrotic remodeling. These findings integrate structural and molecular evidence into a unified pathogenic framework, highlighting the central role of ubiquitin dysregulation in the early initiation of airway fibrosis and providing new mechanistic insight that may inform future therapeutic strategies for BO.

Although this study provides new evidence linking fibrosisrelated gene activation and ubiquitin dysregulation to diacetylinduced bronchiolitis obliterans, several aspects warrant further exploration. Our transcriptomic analysis was conducted on whole-lung tissue, and cell-type-specific contributions to UbC induction and fibrosis require more precise delineation. The observed association between UbC upregulation, fibroblast activation, and extracellular matrix remodeling strongly suggests a central regulatory role for UbC in airway fibrosis. In addition, as the current model reflects early fibrotic remodeling, extending observations to later time points may clarify whether these ubiquitin-related alterations persist and drive chronic airway obstruction. This experiment was conducted as a single exposure series, the model has demonstrated highly consistent histological and transcriptomic outcomes across animals, supporting reproducibility. Future studies will incorporate independent biological replicates to validate the robustness of these findings and examine UbC-related responses across extended time frames. Overall, these findings provide a robust molecular foundation for understanding UbC-mediated pathways in fibrotic airway injury

and establish a basis for future mechanistic and therapeutic investigations.

Collectively, these efforts will refine the mechanistic framework proposed here and may ultimately contribute to the development of novel therapeutic strategies targeting ubiquitin regulation in bronchiolitis obliterans.

5 Conclusion

In conclusion, a single intratracheal instillation of diacetyl (DA) induced characteristic pathological features of bronchiolitis obliterans in rat lungs, including epithelial injury, inflammation, and progressive fibrosis. These structural alterations were accompanied by disrupted ubiquitin regulation and a marked increase in UbC protein expression, suggesting a stress-induced activation of the ubiquitin–proteasome system linked to oxidative injury. The present findings highlight the pivotal role of ubiquitin dysregulation in the early stages of airway fibrosis and provide a molecular foundation for exploring UbC-targeted interventions in the prevention and treatment of bronchiolitis obliterans.

Data availability statement

All data generated or analyzed during this study are included in this published article and its supplementary information files. The raw sequence data reported in this paper have been deposited in the Genome Sequence Archive (Genomics, Proteomics & Bioinformatics 2021) in National Genomics Data Center (Nucleic Acids Res 2021), China National Center for Bioinformation/Beijing Institute of Genomics, Chinese Academy of Sciences (GSA: CRA018830) that are publicly accessible at https://ngdc.cncb.ac.cn/gsa.

Ethics statement

The animal study was approved by the Animal Ethics Committee of the Second Hospital of Shandong University. The study was conducted in accordance with the local legislation and institutional requirements.

Author contributions

HW: Writing – review and editing, Conceptualization, Writing – original draft, Funding acquisition, Formal Analysis, Validation. WJ: Writing – review and editing, Data curation, Writing – original draft, JX: Writing – original draft,

References

Aguilar, P. R., Michelson, A. P., and Isakow, W. (2016). Obliterative bronchiolitis. Transplantation 100 (2), 272–283. PMID: 26335918. doi:10.1097/TP. 0000000000000892

Allen, J. G., Flanigan, S. S., LeBlanc, M., Vallarino, J., MacNaughton, P., Stewart, J. H., et al. (2015). Flavoring chemicals in E-Cigarettes: diacetyl, 2,3-Pentanedione, and

Writing – review and editing, Data curation. YG: Formal Analysis, Writing – review and editing, Writing – original draft. QY: Writing – original draft, Formal Analysis, Writing – review and editing. WG: Supervision, Writing – review and editing, Funding acquisition, Project administration.

Funding

The authors declare that financial support was received for the research and/or publication of this article. This study was supported by Shandong Provincial Natural Science Foundation (No. ZR2020MH002).

Conflict of interest

The authors declare that the research was conducted in the absence of any commercial or financial relationships that could be construed as a potential conflict of interest.

Generative Al statement

The authors declare that no Generative AI was used in the creation of this manuscript.

Any alternative text (alt text) provided alongside figures in this article has been generated by Frontiers with the support of artificial intelligence and reasonable efforts have been made to ensure accuracy, including review by the authors wherever possible. If you identify any issues, please contact us.

Publisher's note

All claims expressed in this article are solely those of the authors and do not necessarily represent those of their affiliated organizations, or those of the publisher, the editors and the reviewers. Any product that may be evaluated in this article, or claim that may be made by its manufacturer, is not guaranteed or endorsed by the publisher.

Supplementary material

The Supplementary Material for this article can be found online at: https://www.frontiersin.org/articles/10.3389/fphar.2025.1671557/full#supplementary-material

SUPPLEMENTARY TABLE \$1

The top 30 differentially expressed genes (DEGs) identified at Day 7 ($|log_2FC|$ ranked), as RNA-seq was performed exclusively at this time point.

acetoin in a sample of 51 products, including fruit-, candy-, and cocktail-flavored E-Cigarettes. *Environ. Health Perspect.* 124, 733–739. doi:10.1289/ehp.1510185

Barker, A. F., Bergeron, A., Rom, W. N., and Hertz, M. I. (2014). Obliterative bronchiolitis. *N. Engl. J. Med.* 370 (19), 1820–1828. PMID: 24806161. doi:10.1056/NEIMra1204664

Buetow, L., and Huang, D. T. (2016). Structural insights into the catalysis and regulation of E3 ubiquitin ligases. *Nat. Rev. Mol. Cell Biol.* 17 (10), 626–642. Epub 2016 Aug 3. PMID: 27485899; PMCID: PMC6211636. doi:10.1038/nrm. 2016.91

- Chaugule, V. K., and Walden, H. (2016). Specificity and disease in the ubiquitin system. *Biochem. Soc. Trans.* 44 (1), 212–227. PMID: 26862208; PMCID: PMC5264512. doi:10.1042/BST20150209
- Chen, Y., Dai, R., Cheng, M., Wang, W., Liu, C., Cao, Z., et al. (2024). Status and role of the ubiquitin-proteasome system in renal fibrosis. *Biomed. Pharmacother.* 178, 117210. Epub 2024 Jul 25. PMID: 39059348. doi:10.1016/j.biopha.2024.117210
- Dastsooz, H., Cereda, M., Donna, D., and Oliviero, S. (2019). A comprehensive bioinformatics analysis of *UBE2C* in cancers. *Int. J. Mol. Sci.* 20 (9), 2228. PMID: 31067633; PMCID: PMC6539744. doi:10.3390/ijms20092228
- Flake, G. P., and Morgan, D. L. (2017). Pathology of diacetyl and 2,3-pentanedione airway lesions in a rat model of obliterative bronchiolitis. *Toxicology* 388, 40–47. Epub 2016 Oct 29. PMID: 27984136; PMCID: PMC5644391. doi:10.1016/j.tox.2016.10.013
- Gloede, E., Cichocki, J. A., Baldino, J. B., and Morris, J. B. (2011). A validated hybrid computational fluid dynamics-physiologically based pharmacokinetic model for respiratory tract vapor absorption in the human and rat and its application to inhalation dosimetry of diacetyl. *Toxicol. Sci.* 123 (1), 231–246. Epub 2011 Jun 24. PMID: 21705714. doi:10.1093/toxsci/kfr165
- Harber, P., Saechao, K., and Boomus, C. (2006). Diacetyl-induced lung disease. *Toxicol. Rev.* 25 (4), 261–272. PMID: 17288497. doi:10.2165/00139709-200625040-00006
- Hubbs, A. F., Fluharty, K. L., Edwards, R. J., Barnabei, J. L., Grantham, J. T., Palmer, S. M., et al. (2016). Accumulation of ubiquitin and Sequestosome-1 implicate protein damage in diacetyl-induced cytotoxicity. *Am. J. Pathol.* 186 (11), 2887–2908. PMID: 27643531; PMCID: PMC5222965. doi:10.1016/j.ajpath.2016.07.018
- Hubbs, A. F., Kreiss, K., Cummings, K. J., Fluharty, K. L., O'Connell, R., Cole, A., et al. (2019). Flavorings-related lung disease: a brief review and new mechanistic data. *Toxicol. Pathol.* 47 (8), 1012–1026. Epub 2019 Oct 23. PMID: 31645208. doi:10. 1177/0192623319879906
- Kerger, B. D., and Fedoruk, M. J. (2015). Pathology, toxicology, and latency of irritant gases known to cause bronchiolitis obliterans disease: does diacetyl fit the pattern? *Toxicol. Rep.* 2, 1463–1472. PMID: 28962489; PMCID: PMC5598164. doi:10.1016/j. toxrep.2015.10.012
- Kimura, Y., and Tanaka, K. (2010). Regulatory mechanisms involved in the control of ubiquitin homeostasis. *J. Biochem.* 147 (6), 793–798. Epub 2010 Apr 23. PMID: 20418328. doi:10.1093/jb/mvq044
- Kreiss, K. (2014). Work-related spirometric restriction in flavoring manufacturing workers. Am. J. Ind. Med. 57 (2), 129–137. Epub 2013 Nov 22. PMID: 24265107; PMCID: PMC4586123. doi:10.1002/ajim.22282
- Kreiss, K. (2017). Recognizing occupational effects of diacetyl: what can we learn from this history? *Toxicology* 388, 48–54. Epub 2016 Jun 17. PMID: 27326900; PMCID: PMC5323392. doi:10.1016/j.tox.2016.06.009
- Krishna, R., Anjum, F., and Oliver, T. I. (2024). "Bronchiolitis obliterans. 2023 Aug 14," in *StatPearls. Treasure Island (FL)* (StatPearls Publishing). PMID: 28722895.
- Landman, S. T., Dhaliwal, I., Mackenzie, C. A., Martinu, T., Steel, A., and Bosma, K. J. (2019). Life-threatening bronchiolitis related to electronic cigarette use in a Canadian youth. *CMAJ* 191 (48), E1321–E1331. Epub 2019 Nov 20. PMID: 31753841; PMCID: PMC6887563. doi:10.1503/cmaj.191402
- Lee, S. Y., Park, S. Y., Lee, S. H., Kim, H., Kwon, J. H., Yoo, J. Y., et al. (2023). The deubiquitinase UCHL3 mediates p300-dependent chemokine signaling in alveolar type II cells to promote pulmonary fibrosis. *Exp. Mol. Med.* 55 (8), 1795–1805. Epub 2023 Aug 1. PMID: 37524875; PMCID: PMC10474292. doi:10.1038/s12276-023-01066-1
- Lynch, J. P., Weigt, S. S., DerHovanessian, A., Fishbein, M. C., Gutierrez, A., and Belperio, J. A. (2012). Obliterative (constrictive) bronchiolitis. *Semin. Respir. Crit. Care Med.* 33 (5), 509–532. Epub 2012 Sep 21. PMID: 23001805. doi:10.1055/s-0032-1325161
- Marinovic, A. C., Zheng, B., Mitch, W. E., and Price, S. R. (2002). Ubiquitin (UbC) expression in muscle cells is increased by glucocorticoids through a mechanism involving Sp1 and MEK1. *J. Biol. Chem.* 277 (19), 16673–16681. Epub 2002 Feb 28. PMID: 11872750. doi:10.1074/jbc.M200501200
- Morgan, D. L., Flake, G. P., Kirby, P. J., and Palmer, S. M. (2008). Respiratory toxicity of diacetyl in C57BL/6 mice. *Toxicol. Sci.* 103 (1), 169–180. Epub 2008 Jan 27. PMID: 18227102; PMCID: PMC2669658. doi:10.1093/toxsci/kfn016
- Morgan, D. L., Jokinen, M. P., Price, H. C., Gwinn, W. M., Palmer, S. M., and Flake, G. P. (2012). Bronchial and bronchiolar fibrosis in rats exposed to 2,3-pentanedione vapors: implications for bronchiolitis obliterans in humans. *Toxicol. Pathol.* 40 (3), 448–465. Epub 2012 Jan 3. PMID: 22215510. doi:10.1177/0192623311431946
- Palmer, S. M., Flake, G. P., Kelly, F. L., Zhang, H. L., Nugent, J. L., Kirby, P. J., et al. (2011). Severe airway epithelial injury, aberrant repair and bronchiolitis obliterans

- develops after diacetyl instillation in rats. PLoS One 6 (3), e17644. PMID: 21464978; PMCID: PMC3064568. doi:10.1371/journal.pone.0017644
- Papiris, S. A., Malagari, K., Manali, E. D., Kolilekas, L., Triantafillidou, C., Baou, K., et al. (2013). Bronchiolitis: adopting a unifying definition and a comprehensive etiological classification. *Expert Rev. Respir. Med.* 7 (3), 289–306. PMID: 23734650. doi:10.1586/ers.13.21
- Perrotta, I., Bruno, L., Maltese, L., Russo, E., Donato, A., and Donato, G. (2012). Immunohistochemical analysis of the ubiquitin-conjugating enzyme UbcH10 in lung cancer: a useful tool for diagnosis and therapy. *J. Histochem Cytochem* 60 (5), 359–365. Epub 2012 Mar 2. PMID: 22388643; PMCID: PMC3351232. doi:10.1369/0022155412439717
- Pickart, C. M., and Fushman, D. (2004). Polyubiquitin chains: polymeric protein signals. *Curr. Opin. Chem. Biol.* 8 (6), 610–616. PMID: 15556404. doi:10.1016/j.cbpa. 2004.09.009
- Radici, L., Bianchi, M., Crinelli, R., and Magnani, M. (2013). Ubiquitin C gene: structure, function, and transcriptional regulation. *Adv. Biosci. Biotechnol.* 4, 1057–1062. doi:10.4236/abb.2013.412141
- Rajsbaum, R., and García-Sastre, A. (2014). Virology. Unanchored ubiquitin in virus uncoating. *Science* 346 (6208), 427–428. PMID: 25342790. doi:10.1126/science.
- Rajsbaum, R., Versteeg, G. A., Schmid, S., Maestre, A. M., Belicha-Villanueva, A., Martínez-Romero, C., et al. (2014). Unanchored K48-linked polyubiquitin synthesized by the E3-ubiquitin ligase TRIM6 stimulates the interferon-IKKe kinase-mediated antiviral response. *Immunity* 40 (6), 880–895. Epub 2014 May 29. PMID: 24882218; PMCID: PMC4114019. doi:10.1016/j.immuni.2014.04.018
- Ryu, H. W., and Ryu, K. Y. (2011). Quantification of oxidative stress in live mouse embryonic fibroblasts by monitoring the responses of polyubiquitin genes. *Biochem. Biophys. Res. Commun.* 404 (1), 470–475. Epub 2010 Dec 7. PMID: 21144824. doi:10. 1016/j.bbrc.2010.12.004
- Ryu, K. Y., Maehr, R., Gilchrist, C. A., Long, M. A., Bouley, D. M., Mueller, B., et al. (2007). The mouse polyubiquitin gene UbC is essential for fetal liver development, cell-cycle progression and stress tolerance. *EMBO J.* 26 (11), 2693–2706. Epub 2007 May 10. PMID: 17491588: PMCID: PMC1888680. doi:10.1038/si.emboi.7601722
- Sauler, M., and Gulati, M. (2012). Newly recognized occupational and environmental causes of chronic terminal airways and parenchymal lung disease. *Clin. Chest Med.* 33 (4), 667–680. PMID: 23153608; PMCID: PMC3515663. doi:10.1016/j.ccm.2012.09.002
- Schachter, E. N. (2002). Popcorn worker's lung. N. Engl. J. Med. 347 (5), 360–361. PMID: 12151475. doi:10.1056/NEJMe020064
- Silva, C. I. S., and Müller, N. L. (2008). Obliterative bronchiolitis. CT of the airways. doi:10.1007/978-1-59745-139-0 13
- Snyder, N. A., and Silva, G. M. (2021). Deubiquitinating enzymes (DUBs): regulation, homeostasis, and oxidative stress response. *J. Biol. Chem.* 297 (3), 101077. Epub 2021 Aug 12. PMID: 34391779; PMCID: PMC8424594. doi:10.1016/j.jbc.2021.101077
- Spratt, D. E., Walden, H., and Shaw, G. S. (2014). RBR E3 ubiquitin ligases: new structures, new insights, new questions. *Biochem. J.* 458 (3), 421–437. PMID: 24576094; PMCID: PMC3940038. doi:10.1042/BJ20140006
- Swatek, K. N., and Komander, D. (2016). Ubiquitin modifications. *Cell Res.* 26 (4), 399–422. Epub 2016 Mar 25. PMID: 27012465; PMCID: PMC4822133. doi:10.1038/cr. 2016.39
- Tsirigotis, M., Zhang, M., Chiu, R. K., Wouters, B. G., and Gray, D. A. (2001). Sensitivity of mammalian cells expressing mutant ubiquitin to protein-damaging agents. *J. Biol. Chem.* 276 (49), 46073–46078. PMID: 11598140. doi:10.1074/jbc. M109023200
- van Ree, J. H., Jeganathan, K. B., Malureanu, L., and van Deursen, J. M. (2010). Overexpression of the E2 ubiquitin-conjugating enzyme UbcH10 causes chromosome missegregation and tumor formation. *J. Cell Biol.* 188 (1), 83–100. PMID: 20065091; PMCID: PMC2812857. doi:10.1083/jcb.200906147
- Villegas-Ruiz, V., and Juarez-Mendez, S. (2016). Data mining for identification of molecular targets in ovarian cancer. *Asian Pac J. Cancer Prev.* 17 (4), 1691–1699. PMID: 27221839. doi:10.7314/apjcp.2016.17.4.1691
- Wang, J., Xie, Y., Bai, X., Wang, N., Yu, H., Deng, Z., et al. (2017). Targeting dual specificity protein kinase TTK attenuates tumorigenesis of glioblastoma. *Oncotarget* 9 (3), 3081–3088. PMID: 29423030; PMCID: PMC5790447. doi:10.18632/oncotarget. 23152
- Wang, J., Kim, S. Y., House, E., Olson, H. M., Johnston, C. J., Chalupa, D., et al. (2021). Repetitive diacetyl vapor exposure promotes ubiquitin proteasome stress and precedes bronchiolitis obliterans pathology. *Arch. Toxicol.* 95 (7), 2469–2483. Epub 2021 May 24. PMID: 34031698; PMCID: PMC8336605. doi:10.1007/s00204-021-03076-2
- Zhang, K., Yuan, H., and Shi, L. (2025). Targeting E3 ubiquitin ligases: a new frontier in idiopathic pulmonary fibrosis treatment. *Front. Immunol.* 16, 1618424. PMID: 40901482; PMCID: PMC12399401. doi:10.3389/fimmu.2025.1618424